Journal of Solid State Chemistry 184 (2011) 1439–1444

Contents lists available at ScienceDirect

Journal of Solid State Chemistry

journal homepage: www.elsevier.com/locate/jssc

Neutron diffraction study of La_4LiAuO_8: Understanding Au^{3+} in an oxide environment

Joshua A. Kurzman [a,*], Stephanie L. Moffitt [a], Anna Llobet [c], Ram Seshadri [a,b]

[a] Department of Chemistry and Biochemistry, University of California, Santa Barbara, CA 93106, United States
[b] Materials Department and Materials Research Laboratory, University of California, Santa Barbara, CA 93106, United States
[c] Los Alamos National Laboratory, Lujan Neutron Scattering Center, MS H805, Los Alamos, NM 87545, United States

ARTICLE INFO

Article history:
Received 6 March 2011
Received in revised form
7 April 2011
Accepted 9 April 2011
Available online 16 April 2011

Keywords:
La_4LiAuO_8
Gold
Neutron diffraction
Maximum entropy method
Bond valence

ABSTRACT

Owing to gold's oxophobicity, its oxide chemistry is rather limited, and elevated oxygen pressures are usually required to prepare ternary and quaternary oxide compounds with gold ions. The Au^{3+} oxide, La_4LiAuO_8, is remarkable both because it can be prepared at ambient pressure in air, and because of its unusual stability toward thermal decomposition and reduction. The structure of La_4LiAuO_8 was established by Pietzuch et al. using single crystal X-ray diffraction [1]. The compound adopts an ordered modification of the Nd_2CuO_4 structure, containing two-dimensional sheets in which AuO_4 square planes are separated from one another by LiO_4 square planes. In light of the meager X-ray scattering factors of Li and O, relative to La and Au, we report here a neutron powder diffraction study of La_4LiAuO_8, definitively confirming the structure. To our knowledge, this is the first reported neutron diffraction study of any stoichiometric oxide compound of gold. *X–N* maps, which make use of nuclear positions obtained from Rietveld refinement of time-of-flight neutron diffraction data and electron densities obtained from synchrotron X-ray powder diffraction data, point to the highly covalent nature of the Au–O bonding in La_4LiAuO_8. This is in good agreement with charge densities and Bader charges obtained from full density functional relaxation of the structure.

1. Introduction

The last 20 or so years have seen a burgeoning interest in gold research in the wake of work by Haruta and co-workers during the late 1980s on carbon monoxide oxidation by nanoparticulate gold [2]. Indeed, the element – traditionally regarded as one of the most inert – displays rich and various catalysis chemistry, much of which is still coming to light. While the excitement about gold often seems to stem from Haruta's work, in a recent review of the pre-1980s gold catalysis literature [3], Bond points out that the first report of CO oxidation by gold was actually published in 1925 [4], and catalytic action by gold was already noted in the 1820s when Dulong and Thenard observed that it catalyzed the decomposition of ammonia [5].

In contrast to the catalytic chemistry of gold, its oxide crystal chemistry appears to be effectively unknown until about 1960 when Hoppe published a brief letter describing the alkali oxoaurates, $AAuO_2$, $A_4Au_2O_5$ (A = K, Rb, Cs), Na_3AuO_3, and Li_5AuO_4 [6]. It was another decade until crystal structure refinements were reported for most of these ternary phases [7], and almost ten additional years before the crystal structure of the binary gold oxide, Au_2O_3, was determined [8]. Most of the Au oxide compounds were discovered in the groups of Hoppe [6,9–15,7], Müller-Buschbaum [16–19], who has published a review on the field [20], and Jansen [21–28]. The quaternary oxide studied here, La_4LiAuO_8, was first prepared by Abbattista et al. [29], and the structure later determined by single crystal X-ray diffraction [1].

The interesting debate on the theme of catalytically active gold species has been with regard to the nature and oxidation state of supported gold clusters or nanoparticles in reactions such as CO oxidation [30–38], water-gas-shift [39–43], and 1,3-butadiene hydrogenation [44–46]. To address the possible catalytic role of Au^{3+}, we recently suggested La_4LiAuO_8 as a model compound for heterogeneous catalysis by isolated Au^{3+} ions [47]. The stability of La_4LiAuO_8 was assessed by thermogravimetry in air, N_2, and 5% H_2 atmospheres, with decomposition (reduction) occurring at 935 °C, 785 °C, and 485 °C, respectively. We have also studied the energetics of La_4LiAuO_8 by high-temperature molten oxide solution calorimetry, and found that the enthalpy of formation is significantly exothermic, with ΔH_f of about -190 kJ mol^{-1} [48]. The other oxoaurates that have been reported to display similar thermal stability are: $LaAuO_3$ (decomposes at 820 °C in air) [27], $La_4Au_2O_9$ (decomposes at 791 °C in Ar) [28], $Ln_4Au_2O_9$ (Ln = Nd, Sm, Eu) (decompose at 700–800 °C in Ar) [23], and Ln_3AuO_6

* Corresponding author.
E-mail address: jkurzman@chem.ucsb.edu (J.A. Kurzman).

0022-4596/$ - see front matter © 2011 Elsevier Inc. All rights reserved.
doi:10.1016/j.jssc.2011.04.021

(*Ln* = Sm, Eu, Gd) (decompose at 700–900 °C in Ar) [24]. The electropositive counter-cations destabilize the O 2*p* states (lower their energy), thereby making oxygen more available to overlap with Au 5*d* orbitals. The stabilization of transition metals in unusually high oxidation states (which also applies to oxophobic elements) by electropositive counter-cations has been discussed by Etourneau et al. [49], and touched upon recently by Sleight [50]. Indeed, in our previous study [47], maximum-entropy electron density restoration of synchrotron X-ray powder diffraction data of La_4LiAuO_8 suggested covalent Au–O bonding, whereas the Li–O interaction was seen to be almost completely ionic.

In light of the absence of neutron diffraction studies on stoichiometric oxide compounds of gold, and to dispel any lingering skepticism that may arise from the difficulty of locating oxygen and lithium by X-ray scattering, we present studies of the structure of La_4LiAuO_8 from simultaneous refinement of of time-of-flight (TOF) neutron and synchrotron X-ray powder diffraction data. In addition to presenting experimentally determined nuclear and electron densities of La_4LiAuO_8, we compare our experimental findings with density functional calculations, including full structure relaxation and Bader charge analysis, demonstrating remarkable agreement between our previous [47] and present scattering studies, and theory.

2. Materials and methods

The preparation of polycrystalline La_4LiAuO_8 by solid-state reaction has been described previously [29,47]. Polycrystalline La_4LiAuO_8 was prepared by solid state reaction between La_2O_3 (Alfa Aesar, 99.99%, pre-heated overnight at 850 °C), Au metal powder (Cerac, 99.95%), and a 50% molar excess of $LiOH \cdot H_2O$ (Cerac, $\geq 98\%$), heated on silver foil in air at 750 °C for a total of 30 h, with five intermittent re-grindings. The as-prepared sample was washed repeatedly in DI H_2O to remove unreacted lithium species. Synchrotron X-ray powder diffraction data was collected at room temperature with an X-ray wavelength of 0.413981 Å at beamline 11-BM at the Advanced Photon Source, Argonne National Laboratory. Time-of-flight (TOF) neutron powder diffraction data was collected at room temperature, with the sample held in a vanadium can, on the HIPD instrument at Los Alamos National Laboratory. The same sample was used for X-ray and neutron diffraction experiments. Rietveld refinements [51] were performed using the GSAS/EXPGUI suite [52,53], and the XND code [54]. Because GSAS cannot accommodate multiple constraints of the same parameter for a given atom – specifically the requirement that the Li and Au occupancies be equal *and* that the sum of the site and anti-site occupancies be one – occupancies refined from the synchrotron X-ray data using the XND code, $\delta = 0.10(1)$, were adopted and fixed in GSAS refinements. Allowing the occupancy parameters for all of the atom positions to float, free from any constraints, led to convergence within about 1% of the nominal stoichiometry $La_4Li_{0.9}Au_{0.1}Au_{0.9}Li_{0.1}O_8$ for simultaneous refinement of both neutron and X-ray data sets. Atomic displacement parameters (ADPs) were modeled isotropically in all refinements, with U_{eq} for Au and Li constrained to the same value in refinement of the X-ray data. In refinements containing the neutron dataset, U_{eq} of Au and Li were allowed distinct values. Attempts to refine the O ADPs anisotropically led to a small but negative (non-physical) value for U_{11}. A so-called "*X*–*N*" ($X-N$) map of the electron density distribution in the unit cell was constructed using RIETAN-FP [55] and PRIMA [56] by performing a maximum entropy method (MEM) reconstruction to the synchrotron X-ray diffraction data with nuclear positions fixed at those obtained from refinement of TOF neutron diffraction data. MEM analysis was performed with the unit cell divided into $64 \times 64 \times 128$ voxels. The application VESTA [57] was used to visualize electron and nuclear densities. Bond valence sums were calculated using the Bond Valence Calculator [58].

First-principle density functional calculations were performed in the VASP package [59,60], which uses a plane-wave basis set to describe the valence electrons. Interaction between the valence and core electrons was described using the projector augmented wave (PAW) approach [61], with cores of [Kr] for lanthanum, [Xe] for gold, and [He] for oxygen. Exchange and correlation were treated with the Perdew–Burke–Ernzerhof [62] (PBE) functional within the generalized gradient approximation (GGA). A cutoff energy of 500 eV was employed, and the Brillouin zone was sampled with 32 irreducible *k*-points using a $8 \times 8 \times 4$ Monkhorst–Pack mesh. Structure relaxation was deemed to have converged when the forces on all the ions were less than 0.01 eV $Å^{-1}$. The atomic charges in the geometry optimized structure were determined using the Bader analysis program [63–66], based on Bader's theory of atoms in molecules (AIM) [67].

3. Results and discussion

La_4LiAuO_8 was prepared in the presence of a 50% molar excess of LiOH. We confirmed previously by ^6Li NMR that washing effectively removes Li species not incorporated into the La_4LiAuO_8 lattice [47]. Excess lithium hydroxide likely serves as a flux in the reaction, primarily improving solid state diffusion and perhaps also moderately promoting the oxidation of gold. While LiOH has the greatest tendency to dissociate amongst the alkali hydroxides, it is also the least effective at stabilizing dissolved peroxides and superoxides, in line with the inability of Li to stabilize peroxides and superoxides in the solid state. Thus, oxidation of the Au^0 starting material is likely to be primarily attributable to the presence of La_2O_3. While the Ln_4LiAuO_8 (*Ln* = Nd, Sm, Eu, Gd) phases are known, only the lanthanum containing phase can be prepared at ambient pressure [68].

Data from the highest resolution TOF neutron detector bank and the synchrotron X-ray powder diffraction pattern, along with corresponding Rietveld refinements from simultaneous refinement of both data sets, are shown in Fig. 1. The synchrotron X-ray data set is divided at a *d*-spacing of 1.5 Å to ease inspection of the fit quality. Structural parameters from simultaneous neutron and X-ray refinement, and refinement of both neutron and X-ray data sets separately, are given in Table 1. In our previous study, we found that the preparation of phase-pure La_4LiAuO_8 powders is difficult to achieve [47]. Even when vast excesses of La_2O_3 and LiOH are used, a small amount of metallic Au is always found to be present. Interestingly, the Au^0 is not the bulk gold of the starting material, but rather nanocrystalline Au particles. Thus, despite thermogravimetric and calorimetric studies that show La_4LiAuO_8 is a particularly stable compound, the material may undergo some degree of surface decomposition. An alternate explanation is that a ternary phase between Li or La and Au may compete with La_4LiAuO_8 during the reaction, decomposing to leave behind nanoparticulate Au. Indeed, the sample studied here contained 1% Au by weight, in addition to another very minor impurity phase. The identity of the other impurity could not be determined, but was not consistent with oxides, hydroxides, or carbonates of La or Li, nor could it be fit by any of the ternary oxides of Li and La, La and Au, or Li and Au. Whereas the Au (111) reflection registered about 2400 counts, the strongest reflection from the unknown impurity registered slightly over 1000 counts. Knowledge of the presence of this phase is enabled by the exceptionally high flux and resolution of the 11-BM diffractometer. No indications of the phase are evident in the neutron data, nor in our previous synchrotron X-ray study in

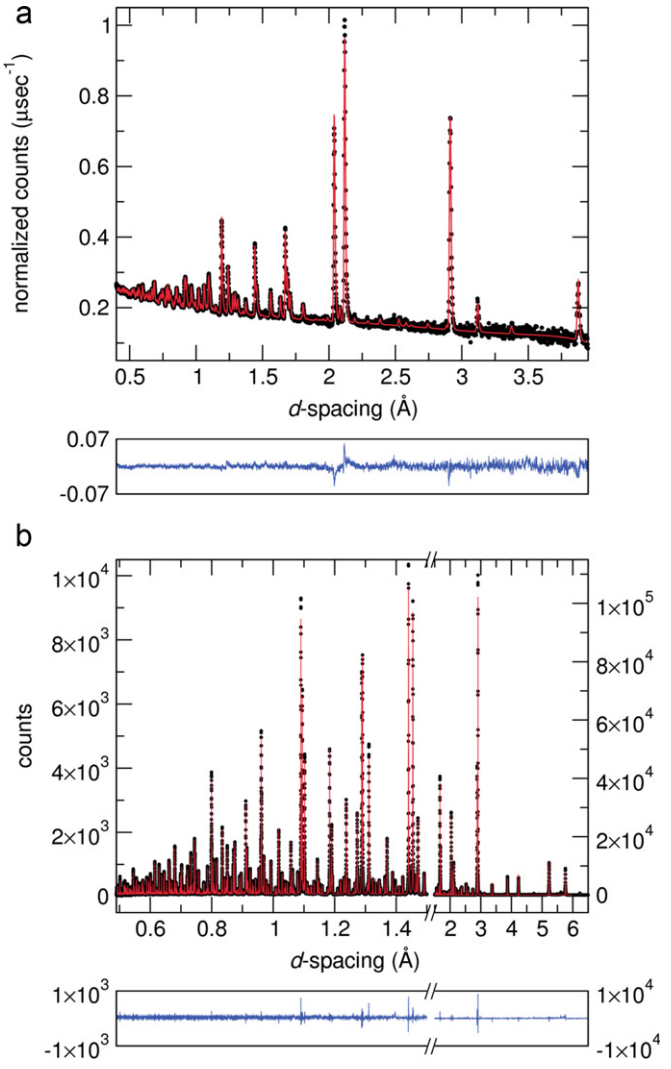

Fig. 1. Rietveld fits from simultaneous refinement of time-of-flight neutron and synchrotron X-ray powder diffraction data. (a) The highest resolution bank of time-of-flight neutron data. (b) Synchrotron X-ray data. The scale of the synchrotron X-ray data is divided at a *d*-spacing of 1.5 Å to facilitate visual inspection of the fit.

which an area detector was used [47], which does not provide the angular resolution attainable at 11-BM.

The introduction of anti-site mixing between Li and Au, designated here as δ when the chemical formula is written $La_4Li_{1-\delta}Au_\delta Au_{1-\delta}Li_\delta O_8$, significantly improved the visual agreement and statistical measures of the Rietveld fits. The necessity to account for mixed site occupancy in the average structure (unit-cell) model is likely due to stacking faults in the layered material. Our previous ^{6}Li NMR study indicated the presence of a single isotropic Li environment, supported by synchrotron X-ray pair distribution function (PDF) analysis in which no evidence for interruptions in the Li–O–Au connectivities were detected [47]. Although Li is effectively X-ray transparent, the large scattering amplitude of Au enables very accurate site-mixing values to be obtained from Rietveld refinement; the absence of any defect-type Au–Au correlations in the real-space PDF thus supports a model in which the LiO_4/AuO_4 layers are pristine, suggesting that the anti-site disorder in the average structure model arises from either faults in registry between some of the layers, or possibly from domain twinning.

Table 1
La_4LiAuO_8, space group *Ammm* (no. 65, setting 3). The atom positions are: La1 (4*i*) at (0,0,*z*), La2 (4*j*) at (1/2,0,*z*), Li (2*b*) at (0,0,1/2), Au (2*d*) at (1/2,0,0), O1 (8*o*) at (*x*,*y*,0) and O2 (8*m*) at (*x*,1/4,1/4). δ refers to the extent of site mixing between Li and Au, when the composition is written $La_4Li_{1-\delta}Au_\delta Au_{1-\delta}Li_\delta O_8$. Isotropic thermal displacement parameters have been multiplied by 100. * denotes cases where δ had to be fixed, as explained in the methods section, and thus no estimated error is given. Agreement statistics for simultaneous refinement of neutron and synchrotron X-ray data: R_{wp} = 3.18%, R_p=3.33%, χ^2 = 4.92. BVS denotes bond valence sum, calculated from nearest neighbor cation-anion distances. BC denotes charge determined by Bader analysis, defined as the number of valence electrons minus the calculated charge.

	N and *X*	Neutron	Synchrotron	DFT
a (Å)	5.76017(1)	5.7601(6)	5.76015(2)	5.7867
b (Å)	5.75984(1)	5.7599(6)	5.75994(2)	5.7863
c (Å)	12.46453(1)	12.4637(1)	12.46451(1)	12.5274
V (Å^3)	413.544(1)	413.521(4)	413.546(1)	419.46
La1, *z*	0.149133(22)	0.14903(8)	0.14924(3)	0.14971
La1, U_{eq}	0.405(6)	0.536(29)	0.427(6)	
La1, BVS	3.17	3.18	3.08	
La1, BC				2.04
La2, *z*	0.350588(23)	0.35137(8)	0.35046(3)	0.35029
La2, U_{eq}	0.412(6)	0.356(28)	0.441(7)	
La2, BVS	3.15	3.11	3.24	
La2, BC				2.04
Li/Au, δ	0.10*	0.10*	0.10(1)	
Li, U_{eq}	0.13(7)	3.1(9)	0.337(6)	
Li, BVS	0.90	0.91	0.85	
Li, BC				0.90
Au, U_{eq}	0.290(6)	0.91(4)	0.337(6)	
Au, BVS	2.77	2.75	2.94	
Au, BC				0.86
O1, *x*	0.25129(26)	0.25051(28)	0.2548(5)	0.25073
O1, *y*	0.24870(26)	0.24854(26)	0.2469(5)	0.24922
O1, U_{eq}	0.766(10)	0.819(10)	0.72(6)	
O1, BVS	1.77	1.78	1.80	
O1, BC				−1.17
O2, *x*	0.24949(25)	0.24894(26)	0.2528(5)	0.24947
O2, U_{eq}	0.559(11)	0.585(9)	0.38(5)	
O2, BVS	2.30	2.28	2.31	
O2, BC				−1.31

It is important to comment on the rather large value of χ^2 obtained for the refinement (simultaneous neutron and X-ray) reported here. The largest contribution to the seemingly poor statistical agreement arises from difficulty in describing the profile shapes, particularly in the synchrotron data. As discussed by Toby [69], large values of χ^2 are apt to occur in refinement of high quality data where the standard uncertainties of the intensities are known to high precision. Small discrepancies are thus of high statistical significance, and can exacerbate statistical measures of fit quality. The visual agreement between the observed and calculated intensities is very strong, however, and comparable statistics were obtained in a LeBail fit to the data, suggesting that the statistical discrepancy arises not from any error in the model per se, but rather from other aspects of the modeling. We note that while the lattice parameters of La_4LiAuO_8 indicate a very minor orthorhombic distortion, it was impossible to obtain a satisfactory LeBail fit in a tetragonal crystal system.

In Fig. 2, a unit-cell depiction of La_4LiAuO_8 is shown (left), along with the nuclear scattering density isosurface reconstructed by Fourier mapping of F_{obs} (middle), and electron density isosurface reconstructed from the synchrotron X-ray dataset by the MEM/Rietveld method using the nuclear positions refined from TOF neutron data (*X–N*, right). The nuclear density isosurface is shown at an absolute value of 0.3 fm Å^{-3}. Li has a negative coherent neutron scattering length, and this is illustrated by the blue surface at the Li positions. Electron density isosurfaces are shown at 1 e Å^{-3}. Inspection of the region between Au and O clearly reveals inter-atomic electron density, consistent with

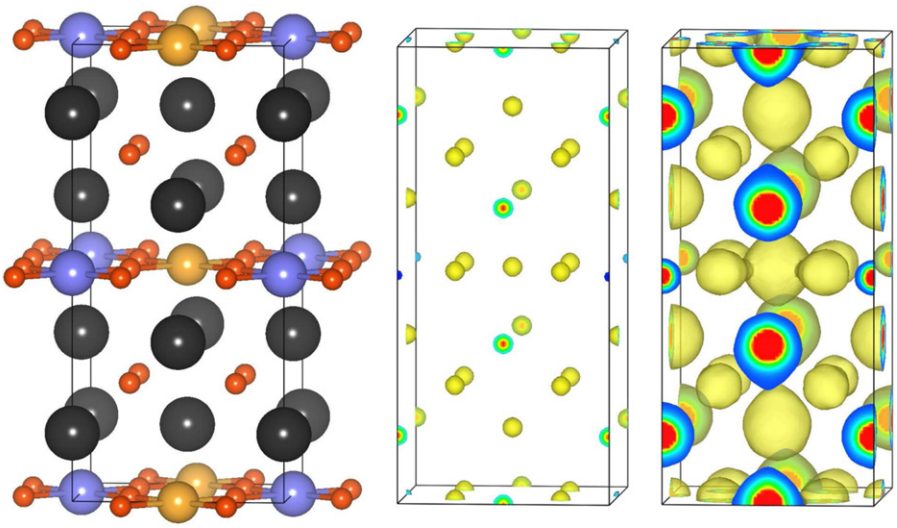

Fig. 2. (Left) Unit cell depiction of La_4LiAuO_8. La is rendered black, Li blue, Au gold, and O orange. (Middle) Observed nuclear scattering densities (F_{obs}), shown at an isosurface level of ± 0.3 fm Å^{-3}. (Right) *X–N* electron density isosurfaces at 1 e Å^{-3}, determined by fixing the nuclear positions at those obtained from refinement of neutron data, and then reconstructed by the MEM/Rietveld method using synchrotron X-ray data. (For interpretation of the references to color in this figure legend, the reader is referred to the web version of this article.)

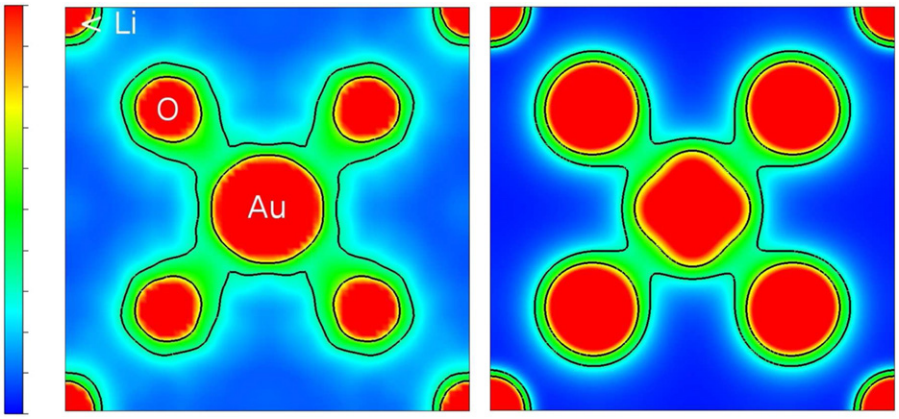

Fig. 3. Electron density distribution on the (002) plane of La_4LiAuO_8. (Left) Experimentally determined from *X–N* reconstruction by the MEM/Rietveld method, shown on a scale from 0 to 3 e Å^{-1}, with contours drawn from 1 to 3 e Å^{-1} at intervals of 1 e Å^{-1}. (Right) Valence charge density from density functional structure relaxation, shown on a scale from 0 to 0.3 e Å^{-1}, with contours drawn from 0.1 to 0.3 e Å^{-1} at 0.1 e Å^{-1} intervals.

covalent Au–O bonding and our previously published result [47]. Excess density on the Li site reflects Li/Au anti-site disorder.

Bond valence sums (BVS) calculated from nearest neighbor cation–anion distances are also given in Table 1. The parameters used to extract the Au^{3+}–O valence contribution were those suggested by I. D. Brown, $R_0=1.89$ and $b=0.37$, available from the CCP14 website [70]. The bond valence parameters for Au^{3+}–O suggested by Bresse and O'Keefe ($R_0=1.833$, $b=0.37$) [71] lead to Au being significantly under-bonded (~ 2.4). Not surprisingly, given the low X-ray scattering amplitudes of Li and O, there are small differences in the Li–O and Au–O bond distances between the X-ray and neutron refinements. Refinement of both neutron and X-ray data sets gave Li–O and Au–O distances of 2.047(2) Å and 2.026(2) Å, respectively, while from the X-ray data alone the Li–O distance is slightly elongated to 2.069(3) Å and the Au–O distance contracted to 2.004(3) Å. All of the bond valence sums are consistent with the expected oxidation states of the respective ions, but O1 appears slightly under-bonded, and O2 somewhat over-bonded. O1 lies in the LiO_4/AuO_4 planes, and receives some of its valence from four long La–O interactions (~ 2.75 Å), while O2 is tetrahedrally coordinated by La at significantly shorter distances (~ 2.39 Å), from which all of its valence sum is derived. As the Au–O distance derived from our neutron refinement should be more reliable than distances found in X-ray diffraction experiments that informed previous estimates of bond valence parameters for Au^{3+}–O^{2-}, we suggest a revised R_0 value of 1.92. Implementing this value only slightly raises the valence sum of O1, but it is likely that the R_0 used for Li, 1.497 [58], is better suited to tetrahedral Li, which is much more commonly encountered. However, we must also note that using the R_0 value of 1.92 to calculate bond valence sums for Au^{3+}–O^{2-} distances determined by X-ray diffraction leads to gold being significantly over-bonded. For example, gold in Au_2O_3 [8] would have a BVS of 3.3. Although it may simply reflect the difficulty in accurately locating oxygen in the presence of heavier elements, it does appear that Au–O distances determined by X-ray diffraction may be systematically under-estimated relative to the inter-atomic nuclear distances.

Full structure relaxation of La_4LiAuO_8 was performed within the generalized gradient approximation using the PBE functional for exchange and correlation, and the structural parameters are given in Table 1. As is common for PBE, the lattice parameters are

slightly overestimated. Forces on all the ions in the relaxed structure are less than 0.01 eV $Å^{-1}$, and nothing suggests an inherent instability of the square planar Li environment, despite this being somewhat uncommon. Bader charges were extracted from the relaxed structure to investigate the bonding character of the different ions. Bader's atoms-in-molecules method provides a way to partition electron density between neighboring atoms, making divisions defined by the critical points of minimal density. Atoms with highly ionic character possess bader charges comparable to their oxidation states, while those that participate in more covalent interactions have depleted Bader charges relative to the oxidation state of the ion. The charges reported in Table 1 were determined by subtracting the calculated charge from the number of valence electrons for each atom. Li, with a charge of 0.90, is clearly very ionic. On the other hand, the calculated charge of Au is just 0.86, suggesting that gold participates in highly covalent bonding with oxygen. Indeed, the charge on O1 (−1.17) is less than that on O2 (−1.31). The electron density distribution in the (002) plane, cutting through a sheet of Li–O–Au connectivities, is compared in Fig. 3 for the *X–N* experimentally reconstructed density and the calculated density. The calculated density is shown for the valence charges only, thus the scales are different for the two representations. It is clear that the calculated distribution fully supports the presence of covalent Au–O bonding in La_4LiAuO_8, as observed experimentally.

4. Conclusions

The remarkably stable complex oxide compound of Au^{3+}, La_4LiAuO_8, has been studied using a combination of time-of-flight neutron and synchrotron X-ray powder diffraction. This is the first reported neutron diffraction study of any pure (rather than lightly substituted) oxide compound of gold. Given the very large atomic number differences between Au and O, neutron scattering is required to draw reliable conclusions with regard to Au^{3+}–O distances. The bonding characteristics, evaluated by maximum entropy reconstruction of the electron densities with nuclear positions fixed at those obtained from refinement of neutron diffraction data, indicate strong covalent bonding between Au and O. This is supported by the use of density functional calculations and Bader charge analysis. The strength of the Au^{3+} stabilization is related to the raising of O 2*p* states by the highly electropositive La^{3+} and Li^{+} counter cations, which enables improved orbital overlap between O 2*p* and Au 5*d* states.

Acknowledgements

We thank the Department of Energy, Office of Basic Energy Sciences for supporting this work through Grant DE-FG02-10ER16081. This work has benefited from the use of the HIPD instrument at the Lujan Center at Los Alamos Neutron Science Center, funded by the DOE Office of Basic Energy Sciences. Los Alamos National Laboratory is operated by Los Alamos National Security LLC under DOE Contract no. DE-AC52-06NA25396. Use of the Advanced Photon Source was supported by the U.S. Department of Energy, Office of Science, Office of Basic Energy Sciences, under Contract no. DE-AC02-06CH11357. This work made use of the computing facilities of the California Nanosystems Institute with facilities provided by NSF Grant no. CHE-0321368 and Hewlett-Packard. The MRL Central Facilities are supported by the MRSEC Program of the NSF under Award no. DMR05-20415; a member of the NSF-funded Materials Research Facilities Network (www.mrfn.org). J.A.K. thanks the ConvEne-IGERT Program (NSF-DGE 0801627) for an Associateship, and Dr. Maosheng Miao, Dr. Kris Delaney, and Dr. Gregg Mills for helpful discussions on density functional methods and Bader analysis. S.L.M. thanks the RISE Program, sponsored by the UCSB MRL, for supporting an internship.

References

[1] W. Pietzuch, S.A. Warda, W. Massa, D. Reinen, Z. Anorg. Allg. Chem. 626 (2000) 113–117.
[2] M. Haruta, T. Kobayashi, H. Sano, N. Yamada, Chem. Lett. 2 (1987) 405–408.
[3] G. Bond, Gold Bull. 41 (2008) 235–241.
[4] W.A. Bone, G.W. Andrew, Proc. R. Soc. A 109 (1925) 459–476.
[5] P.L. Dulong, L.G. Thenard, Ann. Chim. Phys. 23 (1823) 440.
[6] R. Hoppe, Angew. Chem. Intl. Edn. 72 (1960) 584.
[7] H.D. Waselnie, R. Hoppe, Z. Anorg. Allg. Chem. 375 (1970) 43.
[8] P.G. Jones, H. Rumpel, E. Schwarzmann, G.M. Sheldrick, H. Paulus, Acta Crystallogr. B Struct. 35 (1979) 1435–1437.
[9] R. Hoppe, K.H. Arend, Z. Anorg. Allg. Chem. 314 (1962) 4–11.
[10] R. Hoppe, Z. Anorg. Allg. Chem. 630 (2004) 2384–2392.
[11] H. Klassen, R. Hoppe, Naturwissenschaften 63 (1976) 387.
[12] H. Klassen, R. Hoppe, Z. Naturforsch. B. 36 (1981) 1395–1399.
[13] J. Schneider, R. Hoppe, Z. Anorg. Allg. Chem. 574 (1989) 54–64.
[14] G. Wagner, R. Hoppe, Z. Anorg. Allg. Chem. 537 (1986) 115–122.
[15] H.D. Waselnie, R. Hoppe, Z. Anorg. Allg. Chem. 359 (1968) 36.
[16] J. Weinreich, H. Müller-buschbaum, Z. Anorg. Allg. Chem. 617 (1992) 27–30.
[17] J. Weinreich, H. Müller-buschbaum, J. Alloys Compd. 184 (1992) 187–193.
[18] J. Weinreich, H. Müller-buschbaum, J. Alloys Compd. 186 (1992) 105–109.
[19] J. Weinreich, H. Müller-buschbaum, Z. Anorg. Allg. Chem. 619 (1993) 537–539.
[20] H. Müller-Buschbaum, Z. Anorg. Allg. Chem. 628 (2002) 2559–2584.
[21] C. Feldmann, M. Jansen, J. Chem. Soc. Chem. Comm. (1994) 1045–1046.
[22] C. Feldmann, M. Jansen, Z. Anorg. Allg. Chem. 621 (1995) 201–206.
[23] C. Figulla-Kroschel, M. Jansen, Z. Anorg. Allg. Chem. 626 (2000) 2178–2184.
[24] C. Figulla-Kroschel, J. Nuss, M. Jansen, Z. Anorg. Allg. Chem. 627 (2001) 439–444.
[25] J. Geb, M. Jansen, J. Solid State Chem. 122 (1996) 364–370.
[26] G. Kramer, M. Jansen, J. Solid State Chem. 118 (1995) 247–253.
[27] M. Ralle, M. Jansen, J. Solid State Chem. 105 (1993) 378–384.
[28] M. Ralle, M. Jansen, J. Alloys Compd. 203 (1994) 7–13.
[29] F. Abbattista, M. Vallino, D. Mazza, J. Less-Common Metals 110 (1985) 391–396.
[30] J. Guzman, B. Gates, J. Am. Chem. Soc. 126 (2004) 2672–2673.
[31] C. Costello, J. Guzman, J. Yang, Y. Wang, M. Kung, B. Gates, H. Kung, J. Phys. Chem. B 108 (2004) 12529–12536.
[32] V. Schwartz, D. Mullins, W. Yan, B. Chen, S. Dai, S. Overbury, J. Phys. Chem. B 108 (2004) 15782–15790.
[33] R. Zanella, S. Giorgio, C. Shin, C. Henry, C. Louis, J. Catal. 222 (2004) 357–367.
[34] J. Fierro-Gonzalez, B. Gates, J. Phys. Chem. B 108 (2004) 16999–17002.
[35] J.H. Yang, J.D. Henao, M.C. Raphulu, Y.M. Wang, T. Caputo, A.J. Groszek, M.C. Kung, M.S. Scurrell, J.T. Miller, H.H. Kung, J. Phys. Chem. B 109 (2005) 10319–10326.
[36] G.J. Hutchings, M.S. Hall, A.F. Carley, P. Landon, B.E. Solsona, C.J. Kiely, A. Herzing, M. Makkee, J.A. Moulijn, A. Overweg, J.C. Fierro-Gonzalez, J. Guzman, B.C. Gates, J. Catal. 242 (2006) 71–81.
[37] N. Weiher, E. Bus, L. Delannoy, C. Louis, D. Ramaker, J. Miller, J. van Bokhoven, J. Catal. 240 (2006) 100–107.
[38] J.C. Fierro-Gonzalez, J. Guzman, B.C. Gates, Topics Catal. 44 (2007) 103–114.
[39] Q. Fu, H. Saltsburg, M. Flytzani-Stephanopoulos, Science 301 (2003) 935–938.
[40] Z.P. Liu, S.J. Jenkins, D.A. King, Phys. Rev. Lett. 94 (2005).
[41] Q. Fu, W.L. Deng, H. Saltsburg, M. Flytzani-Stephanopoulos, Appl. Catal. B Environ. 56 (2005) 57–68.
[42] D. Tibiletti, A. Amieiro-Fonseca, R. Burch, Y. Chen, J.M. Fisher, A. Goguet, C. Hardacre, P. Hu, A. Thompsett, J. Phys. Chem. B 109 (2005) 22553–22559.
[43] W.D. Williams, M. Shekhar, W.-S. Lee, V. Kispersky, W.N. Delgass, F.H. Ribeiro, S.M. Kim, E.A. Stach, J.T. Miller, L.F. Allard, J. Am. Chem. Soc. 132 (2010) 14018–14020.
[44] X. Zhang, H. Shi, B. Xu, Angew. Chem. Intl. Edn. 44 (2005) 7132–7135.
[45] X. Zhang, H. Shi, B.-Q. Xu, Catal. Today 122 (2007) 330–337.
[46] Y. Guan, E.J.M. Hensen, Phys. Chem. Chem. Phys. 11 (2009) 9578–9582.
[47] J.A. Kurzman, X. Ouyang, W.B. Im, J. Li, J. Hu, S.L. Scott, R. Seshadri, Inorg. Chem. 49 (2010) 4670–4680.
[48] T. Z. Forbes, J. A. Kurzman, R. Seshadri, A. Navrotsky, J. Mater. Res., accepted for publication.
[49] J. Etourneau, J. Portier, F. Menil, J. Alloys Compd. 188 (1992) 1–7.
[50] A.W. Sleight, Prog. Solid State Chem. 37 (2009) 251–261.
[51] H. Rietveld, J. Appl. Crystallogr. 2 (1969) 65.
[52] A.C. Larson, R.B. Von Dreele, Los Alamos National Laboratory Report LAUR 86-748, 2000.
[53] B.H. Toby, J. Appl. Crystallogr. 34 (2001) 210–213.
[54] J.-F. Bérar, P. Garnier, NIST Spec. Publ. 846 (1992) 212.
[55] F. Izumi, K. Momma, Solid State Phenom. 130 (2007) 15–20.
[56] F. Izumi, R.A. Dilanian, Transworld Res. Network 3 (2002) 699–726.
[57] K. Momma, F. Izumi, J. Appl. Crystallogr. 41 (2008) 653–658.

[58] C. Hormillosa, S. Healy, T. Stephen, I.D. Brown ⟨http://ccp14.ac.uk⟩, 1993.
[59] G. Kresse, J. Hafner, Phys. Rev. B 49 (1994) 14251.
[60] G. Kresse, J. Furthmüller, Phys. Rev. B 54 (1996) 11169.
[61] P.E. Blöchl, Phys. Rev. B (1994) 17953.
[62] J.P. Perdew, K. Burke, M. Ernzerhof, Phys. Rev. Lett. 77 (1996) 3865.
[63] ⟨http://theory.cm.utexas.edu/vtsttools/bader⟩.
[64] G. Henkelman, A. Arnaldsson, H. Jónsson, Comput. Mater. Sci. 34 (2006) 354–360.
[65] E. Sanville, S.D. Kenny, R. Smith, G. Henkelman, J. Comp. Chem. 28 (2007) 899–908.
[66] W. Tang, E. Sanville, G. Henkelman, J. Phys. Condens. Matter 21 (2009) 084204.
[67] R.F.W. Bader, Atoms in Molecules: A Quantum Theory, Oxford University Press, Oxford, 1990.
[68] F. Tresse, G. Demazeau, J.P. Sanchez, L. Fournes, K.S. Suh, J. Solid State Chem. 103 (1993) 95–104.
[69] B.H. Toby, Powder Diffr. 21 (2006) 67–70.
[70] ⟨http://www.ccp14.ac.uk/ccp/web-mirrors/i_d_brown/⟩.
[71] N.E. Brese, M. O'Keeffe, Acta. Cryst. B 47 (1991) 192–197.